A Computational Framework for Multi-Scale Simulations of Weakly Ionized Plasmas

Final Report

by

**V.I.Kolobov, R.R. Arslanbekov,
C. Wichaidit, W.N.G. Hitchon and V.F.Kovalev**

June 30, 2008   **CFDRC Report: 8840-03**

REPORT DOCUMENTATION PAGE

1. REPORT DATE *(DD-MM-YYYY)*	2. REPORT TYPE	3. DATES COVERED *(From - To)*
6/30/08	Final	9/1/07 – 6/30/08

4. TITLE AND SUBTITLE
A Computational Framework for Multi-Scale Simulations of Weakly Ionized Plasmas

5a. CONTRACT NUMBER
FA9550-07-C-0069

5b. GRANT NUMBER

5c. PROGRAM ELEMENT NUMBER

6. AUTHOR(S)
V.I.Kolobov, R.R. Arslanbekov,
C. Wichaidit, W.N.G. Hitchon

and V.F.Kovalev

5d. PROJECT NUMBER

5e. TASK NUMBER

5f. WORK UNIT NUMBER

7. PERFORMING ORGANIZATION NAME(S) AND ADDRESS(ES)
CFD Research Corporation
215 Wynn Drive
Huntsville, AL 35016

8. PERFORMING ORGANIZATION REPORT NUMBER
8840

9. SPONSORING / MONITORING AGENCY NAME(S) AND ADDRESS(ES)
Air Force Office of Scientific Research
875 North Randolph Street
Suite 325, Room 3112
Arlington, VA 22203

10. SPONSOR/MONITOR'S ACRONYM(S)

11. SPONSOR/MONITOR'S REPORT NUMBER(S)

12. DISTRIBUTION / AVAILABILITY STATEMENT
Distribution A

13. SUPPLEMENTARY NOTES

14. ABSTRACT
The goal of this STTR project is to develop a unified computational framework integrating adequate physical models for simulating complex non-equilibrium plasmas. The project aims to classify possible scenarios of plasma dynamics and develop general recipes for clustering phase space into sub-domains evolving at different scales and efficiently solve the dynamics for each scale. During Phase I, we developed a methodology to apply methods of Invariant Manifolds and the Renormalization Group for reduced description of plasma kinetics and the transition from micro to macro. We have tested state-of-the-art deterministic Eulerian and Lagrangian kinetic solvers (Vlasov, Fokker-Planck, Boltzmann), investigated new algorithms (such as adaptive mesh in velocity space) and implemented basic plasma capabilities within the Adaptive Mesh and Algorithm Refinement framework. We prepared Phase II work plan where the proposed methodology could be fully developed and implemented in the next generation software for multi-scale plasma simulations. The new capabilities would be valuable for low-pressure weakly-collisional plasma systems with stochastic electron heating and anomalous skin effect, and for high-pressure discharges with runaway electrons, e-beams, sparks and streamers.

15. SUBJECT TERMS
Multi-Scale Simulations, Weakly Ionized Plasmas, Renormalization Group, Slow Invariant Manifolds, Particle kinetics, Boltzmann equation, Fokker-Planck, Stochastic Heating

16. SECURITY CLASSIFICATION OF:			17. LIMITATION OF ABSTRACT	18. NUMBER OF PAGES	19a. NAME OF RESPONSIBLE PERSON Dr Fariba Fahroo
a. REPORT Unclassified	**b. ABSTRACT** Unclassified	**c. THIS PAGE** Unclassified			**19b. TELEPHONE NUMBER** *(include area code)*

TABLE OF CONTENTS

LIST OF FIGURES

EXECUTIVE SUMMARY

The goal of this project is to develop a unified computational framework for multi-scale simulations of weakly-ionized non-equilibrium plasmas. This Final Report for Phase I covers the performance period from September 1, 2007 through June 30, 2008. The main results of the work can be summarized as follows

- We have investigated methods of Renormalization Group and Slow Invariant Manifolds in application to plasma modeling. Using the point symmetry group for the Vlasov-Maxwell system, we obtained exact solutions for the dynamics of collisionless plasma. The interpretation of the solutions in terms of invariants of the group transformation and invariant manifolds was achieved – the particle distribution functions were related to invariants of the group transform. The road towards obtaining approximate symmetries due to small parameter (electron/ion mass ratio) in the plasma was outlined. We prepared detailed work plan for application of these methods during Phase II research.
- We have tested different Eulerian and semi-Lagrangian kinetic solvers for collisionless plasmas. An efficient high-order Vlasov-Poisson solver has been demonstrated for self-consistent simulation of a collisionless boundary layer. Better understanding of the collisionless particle kinetics in a DC sheath was achieved as reflected in the book chapter submitted for publication.
- We have developed a local Boltzmann solver with adaptive mesh in velocity space and tested this solver for simple collision integrals describing electron and ion collisions in weakly ionized plasmas.
- We have developed hydrodynamic models of plasmas with octree based dynamically adaptive Cartesian mesh and demonstrated the model capabilities for streamer simulations.
- The paper "Streamer Simulations with Dynamically Adaptive Cartesian Mesh" was prepared and accepted for publication in a special issue of IEEE Transactions on Plasma Science devoted to "Images in Plasma Physics".

1. APPLICATION OF INVARIANT MANIFOLD AND RENORMALIZATION GROUP METHODS TO PLASMA MODELING

The renormalization group (RG) method has been recently demonstrated as a powerful tool for reduction of evolution equations in terms of <u>invariant manifolds</u>. It was recognized [1] that the reduction of evolution equations is a natural extension of the well-known asymptotic method by Krylov, Bogoliubov and Mitropolski for nonlinear oscillator – the later is in fact an RG theory although the term RG is not used. Using this methodology, the Boltzmann equation was derived as an RG equation [2], the Navier-Stokes equations were derived from the Boltzmann equation [3], and stable post-Navier-Stokes equations have been obtained [4] instead of the unstable Burnett equations. For a classical viscous flow problem, the RG calculations have lead to a new prediction for the drag coefficient, which can reproduce and surpass the results of matched asymptotics [5].

1.1 Slow Invariant Manifolds

The problem of model reduction in physical kinetics was recognized as a problem of time separation and construction of slow invariant manifolds. To illustrate these notations, consider an n-dimensional dynamical system governed by the evolution equation

$$\frac{d\mathbf{W}}{dt} = \mathbf{F}(\mathbf{W}, t) \qquad (1)$$

When the dynamics is reduced to an m-dimensional system ($m<n$), the vector $\mathbf{W}(t)$ approaches a well–defined m-dimensional manifold M embedded in the n-dimensional phase space (see Figure 1). The geometrical object M is called an attractive manifold. If after some time $\mathbf{W}(t)$ is confined in the manifold M, then M is called an invariant manifold. Furthermore, if the dynamics on M is slow, M is called a slow manifold. There is no explicit definition of slow invariant manifolds without explicit small parameter in the system. It was demonstrated how RG method helps construct invariant manifolds and give reduced dynamics on them [3]. The concept of invariant manifolds for physical and chemical kinetics was explicitly developed very recently [6,7].
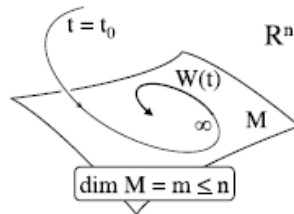
Figure 1.   Illustration of the reduced dynamics. The dynamic variable W(t) approaches to and after some time is eventually confined in the manifold M of lower dimensionality.

1.2 Collisionless Plasma

During Phase I, we have studied how the RG and invariant manifold concepts can be applied to modeling weakly ionized plasmas. We first tried to apply strict results of quasi-neutral plasma theory to interpret dynamics of the plasma-wall transition layer (presheath in CCP, and skin layer in ICP). The analytical expression for the spatio-temporal evolution of the distribution function of electron and ions having initial Gaussian distribution in space and Maxwellian distribution in velocities has been obtained by RG methods in the form

$$f^e = \frac{n_{e0}}{\sqrt{2\pi}\,v_{Te}} \exp\left[-\frac{1+\tau^2}{v_{Te}^2}\left(\frac{(v-u)^2}{2} - \frac{(1+m/M)}{1-v_{Ti}^2/v_{Te}^2}\frac{e\Phi}{m}\right)\right],$$ (2a)

$$f^i = \frac{n_{i0}}{\sqrt{2\pi}\,v_{Ti}} \exp\left[-\frac{1+\tau^2}{v_{Ti}^2}\left(\frac{(v-u)^2}{2} + \frac{(1+\mu^2)}{1-v_{Te}^2/v_{Ti}^2}\frac{e\Phi}{m}\right)\right],$$ (2b)

where the local mean velocity of the plasma u and the electric potential Φ are defined as

$$u = c_s\frac{\varsigma\tau}{1+\tau^2}, \qquad \Phi = -\frac{\varsigma^2}{2e(1+\tau^2)^2}\frac{T_e - \mu^2 T_i}{(1+\mu^2)}.$$

Here $\tau = \Omega t$, $\varsigma = x/L$, $\mu = \sqrt{m/M}$, $c_s = \sqrt{(T_i + T_e)/(M+m)}$ is the sound velocity based on the initial temperatures of electron and ions, $\Omega = c_s/L$, and L is a characteristic scale of plasma non-uniformity (not necessarily equal to the Debye radius r_{De}). This solution is valid for arbitrary ratio of the electron and ion mass, m/M, and arbitrary values of the temperatures, T_e and T_i.

The analytical solution (2) describes many features observed in our simulations of the collisionless plasma-wall transition layer (see below) and results of other authors. In particular, during the time evolution of the initial perturbation, a shift of the mean velocity of electron and ions takes place, and the temperature of ions decreases. Due to the difference of electron and ion mass, $M > m$, ion acceleration is more pronounced since for the thermal velocities $v_{Ti} < v_{Te}$, and the electron acceleration is negligible.

During Phase I, we obtained approximate solutions of unsteady Vlasov-Maxwell system using RG algorithms and slow invariant manifolds. We considered one-dimensional system described by the system of kinetic equations

$$\frac{\partial f^\alpha}{\partial t} + v_\alpha\frac{\partial f^\alpha}{\partial x} + \frac{e_\alpha E}{m_\alpha}\frac{\partial f^\alpha}{\partial v_\alpha} = 0 \qquad \alpha = e, i$$ (3)

with additional equations for the electric field

$$\frac{\partial E}{\partial t} + 4\pi j = 0, \qquad \frac{\partial E}{\partial x} - 4\pi\rho = 0,$$ (4)

and nonlocal material relations

$$\frac{\partial\rho}{\partial t} + \frac{\partial j}{\partial x} = 0, \qquad \rho = \sum_\alpha e_\alpha\int f^\alpha dv_\alpha, \qquad j = \sum_\alpha e_\alpha\int f^\alpha v_\alpha dv_\alpha$$ (5)

We obtained solutions of this system for several cases described below.

Example 1. This case corresponds to generalization of the quasineutral solution (2) for non-zero initial velocity of the plasma constituents having Maxwellian velocity distribution functions. Such a solution can be obtained by applying Galilean transformation to the solution obtained previously. From the physical stand point this operation is equivalent to transformation to a moving reference frame, obtaining solution in this frame, and then returning to the laboratory reference frame. The velocity distribution functions and electric field in the plasma are given by

$$f^{\alpha} = \frac{n_{\alpha 0}}{\sqrt{2\pi}v_{T\alpha}} \exp\left[-\frac{1+\tau^2}{2v_{T\alpha}^2}\left(v_{\alpha} - \frac{c_s\tau\zeta + u}{1+\tau^2} \right)^2 - \frac{(\zeta - u\tau/c_s)^2}{2(1+\tau^2)^2} \right] \tag{6a}$$

$$E = \frac{m_e}{e_e L}\frac{(\zeta - u\tau/c_s)(v_{Te}^2 - v_{Te}^2)}{(1+\tau^2)^2(1+m_e/m_i)}, \tag{6b}$$

It follows from this solution that the mean particle velocity at x=0, which is equal to u at t=0, decrease monotonically with increasing time t. The particle density reaches maximum value at the point $\zeta = u\tau/c_s$, which is moving with time. It is exactly at this point that mean velocity keeps its initial value, u. In fact, the solution (6) describes a localized perturbation moving across the plasma with velocity u.

The solution (6) can be obtained by other means. An alternative approach consists in seeking a solution to kinetic equations that is invariant with respect to a group of local transformations with a generator, which appears as a linear combination of generators of space and time translations and the projective group generator.

The solution (6) is a particular case of a more general solution, which does not assume Maxwellian VDF. In the general case, the dependence of the electric field on spatial coordinate may deviate from the linear dependence (6b). This general solution has the form

$$f^{\alpha} = F^{\alpha}(I^{\alpha}) \quad I^{\alpha} = \frac{1+\tau^2}{2}\left(v_{\alpha} - \frac{c_s\tau\zeta + u}{1+\tau^2} \right)^2 + \frac{(c_s\zeta - u\tau)^2}{2(1+\tau^2)^2} + \frac{e_{\alpha}}{m_{\alpha}}\Phi(J) \tag{7a}$$

$$E = -\frac{1}{(1+\tau^2)^{3/2}}\frac{d\Phi}{dJ}, \quad J = \frac{(c_s\zeta - u\tau)}{\sqrt{1+\tau^2}}, \tag{7b}$$

The dependence of $\Phi(J)$ is determined by the initial VDFs of the particles and by the condition of plasma quasineutrality. The quantities I^{α} and J in (7) are invariants of the group generator constructed from the generators of time and space translations and the projective group generator. The VDFs do not change under group transformation, i.e. they remain invariant, and their relation to the initial VDFs expressed through I^{α} and J defines an invariant manifold corresponding to the solution of the problem.

Example 2. As shown in the previous example, the group of Galilean transformations transforms any solution of the kinetic equations with zero mean velocity to a solution with non-zero mean velocity. As stated above, one can obtain the same solution by an alternative approach consists in seeking a solution to kinetic equations invariant under the local transformation group with a generator, which is a linear combination of generators of time and space translations; in the general case one can also add the generator of the Galilean group. Since all these group generators are admitted by the original Vlasov-Maxwell system without quasineutrality assumption used for obtaining (6), the solution (8) below is valid for arbitrary

relation between the Debye length and the characteristic spatial scale of the plasma

$$f^\alpha = F^\alpha(C^\alpha) \qquad C^\alpha = \frac{1}{2}\left(v_\alpha - u - at\right)^2 + a\Lambda + \frac{e_\alpha}{m_\alpha}\Phi(\Lambda), \tag{8a}$$

$$E = -\frac{d\Phi}{d\Lambda}, \qquad \Lambda = x - ut - \frac{at^2}{2}, \tag{8b}$$

The dependence of $\Phi(\Lambda)$ is found from the initial VDFs with the help of Poisson equation. The solution (8) is a stationary solution of the Vlasov kinetic equations obtained in a reference frame, which moves with initial velocity u and acceleration a. The solution (8) has similar group interpretation as the solution (7), namely C^α and Λ are invariants of the corresponding group generator, which describes the solution to the problem.

The obtained solutions to the one-dimensional Vlasov-Maxwell system are quite obvious from the physical standpoint and thus could be obtained earlier. However, specific solutions to particular problems could be very useful from different points of view. In particular, the developed procedure can be applied to two-component plasmas with prescribed ion motion. The ions can be assumed immobile with given distribution of density, or moving in space with a given velocity. The corresponding expressions can be obtained from the general formulas.

It appears to be difficult to obtain general solutions for arbitrary initial/boundary conditions. However, using the concept of slow invariant manifolds, one can expect to construct an approximate symmetry (RG type) for the Vlasov-Maxwell system, which would allow one to construct solutions for quite arbitrary initial conditions. However, such a procedure would require serious research work.

1.3   Collisional Plasma

During Phase I, we have also studied how invariant manifold methods could be used for reduced description of weakly ionized plasmas with collisions among particles. The difference between scattering rate and the energy loss rate for electrons moving in a neutral gas under effect of external electric field could be utilized for the reduced description of electron kinetics. For slow electrons with energies less than the excitation potential of atoms (~10 eV), scattering dominates over energy loss. For these electrons, the reduced description is possible along the following lines: Boltzmann kinetic equation $\rightarrow$ two-term Spherical Harmonics Expansion (Fokker-Planck Equation), nonlocal approach $\rightarrow$ hydrodynamic model. For fast electrons, the relative importance of scattering and energy loss can be opposite compared to slow electrons. For fast electrons, small angle scattering dominates resulting in electron beams and runaway electrons in high electric field. We anticipate that the Invariant Manifolds and RG methods can be applied for the renormalization of the Boltzmann collision integral and reduced description of collisions in terms of nonlocal friction force that depends on the distribution function.

We have identified several small parameters that can be used for reduced description of the system. These are
- the ratio of electron to ion(atom) mass m_e / m_a
- the ratio of plasma to gas density, $\eta = n_e / N$ (ionization degree)
- the ratio of inelastic to elastic collision frequencies for electrons, v^* / v.

The first one is probably the most important and defines key features of gas discharge physics. As a result of the large difference between the electron and atom mass, electrons respond nearly adiabatically to changes of the external electromagnetic fields, and plasma shields the fields with the (fast) electron time scale. The ion transport and ionization processes occur with (slow) ion time scale. Collisionless invariants (such as total energy (kinetic plus potential)) are important characteristics of the Vlasov-Maxwell system. Small deviations from the adiabatic electron motion can be responsible for the collisionless (stochastic) electron heating – the concept proposed for detailed Phase II studies.

Small ratio of inelastic to elastic collision frequencies for electrons at energies of the order of the excitation potential of atoms (~10 eV) is another important parameter enabling reduced description of electron kinetics in gas discharges. As a result of $m_e / m_a \Box\ 1$ and $v^* / v \Box\ 1$, the reduced description of electrons can proceed along the following lines: Boltzmann Transport Equation -> two-term Spherical Harmonics Expansion (Fokker-Planck Equation), nonlocal approach -> hydrodynamic model (see Figure 2). The Fokker-Planck approach to simulation of electron kinetics in collisional gas discharge plasmas was implemented in the commercial software for plasma simulations developed at CFDRC [8]. Many aspects of the kinetic theory of gas discharges [9] can be interpreted in terms of invariant manifolds. In particular, the procedure of spatial averaging of Bernstein-Holstein-Tsendin for calculation of the electron distribution function in DC and RF discharges (nonlocal approach) can be recognized as a constructive method for creating slow invariant manifold for electron kinetics.

$$6\,D : f(\mathbf{v,r},t)$$
Boltzmann Transport Equation
$$\frac{\partial f}{\partial t} + \nabla_r \cdot (\mathbf{v}f) + \nabla_v \cdot (\frac{\mathbf{F}}{m}f) = Q$$

$vt > \lambda$ velocity correlation time

$$4\,D : f_0(\mathbf{v,r},t)$$
Fokker-Planck Equation
$$\frac{\partial f_0}{\partial t} + \nabla \cdot \Gamma = Q_0(f_0)$$
$$\Gamma_\alpha = V_\alpha f_0 + D_{\alpha\beta}\frac{\partial f_0}{\partial x_\beta} \quad \alpha,\beta = 1...4$$

$ut > \lambda$ energy correlation time

$$3\,D : n(\mathbf{r},t)$$
Drift-Diffusion model
$$\frac{\partial n}{\partial t} + \nabla \cdot (\mathbf{u}n - D\nabla n) = n v_i$$
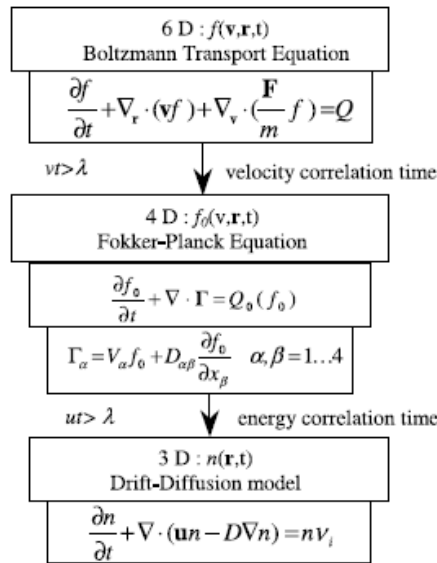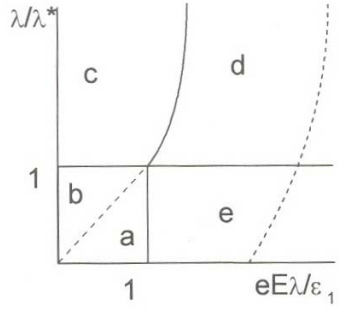
Figure 2.   *A hierarchy of transport models for electrons (from [8])*

For fast electrons, the relative importance of scattering and energy loss can be quite opposite compared to slow electrons. Possible scenarios of EDF formation in a steady electric field *E* for arbitrary rates of scattering and deceleration depicted qualitatively in Figure 3 taken from Ref. 10.

Figure 3   Electron kinetics in external electric field for arbitrary ratios of scattering and deceleration

In the domain *a* both the EDF body and its tail are almost isotropic. The random walk in energy occurs with a step $eE\lambda$, which is small with respect to the EDF characteristic scale ε_1, so one can use the concept of **diffusion in energy** with a diffusion coefficient $D_\varepsilon(v) = (eE\lambda)^2 v/3$. In the domain *b* the energy loss can be treated as quasi-elastic and the distinction between the EDF body and tail disappears.   In the domain *c* the random walk step $eE\lambda$ is small, therefore, the EDF body can be approximated by an isotropic "pipe-line" EDF. In the tail, however, inelastic collisions are very frequent, resulting in a large anisotropy with no electrons moving against the field. In the domain *d*, both the EDF body and tail are strongly anisotropic, and a needle-like EDF along the electric field is formed at energies $w > \varepsilon_1$. A small isotropic halo from elastically scattered electrons contains a small fraction of the total number of electrons. Fast electrons experience small angle scattering and can penetrate deeply into a dense gas producing non-local ionization in the areas with no electric field. The problem of fast electron kinetics in atmospheric pressure plasmas has recently attracted increased attention due to numerous technological applications. We have previously developed simplified models for the fast electron transport and have identified the problem of runaway electrons as a target area for Phase II research. It is anticipated that the Invariant Manifolds and RG methods can also be applied for the renormalization of the Boltzmann collision integral and reduced description of collisions in terms of nonlocal friction force that depends on the distribution function. An example of such a description can be found in [11].

6

2. KINETIC SOLVERS FOR COLLISIONLESS PLASMAS

We have tested accuracy and performance of several Eulerian and semi-Lagrangian kinetic solvers. We have applied a high-order Vlasov-Poisson solver for self-consistent simulation of a boundary layer in collisionless plasma.

2.1 Eulerian Kinetic Solvers

Three Vlasov solvers have been tested for a simple case related to DC sheath in gas discharge plasmas. The first solver is an extension of the UFS kinetic solver [12] with added electric force. The second solver was generously provided by Dr. Shoucri [13]. The third solver is the Convective Scheme solver described in [14]. We considered electric field in the form

$$E(x) = \begin{cases} A(s_m - x)/s_m, & 0 < x < s_m \\ 0 & x > s_m \end{cases} \tag{9}$$

which corresponds to the potential $\varphi(x) = -As_m(1 - x/s_m)\left[1 - (1 + x/s_m)/2\right]$. The particles are injected at $x = s_m$ with a velocity distribution function $f(v_x, v_y) = \exp\left(-\left(v_x - V_0\right)^2/2\right)\exp\left(-v_y^2/2\right)$ and either accelerated or decelerated by the electric field in the sheath (depending on sign of the electric charge). The analytical solution for the VDF has been found in the form

$$f(v_x, v_y) = \exp\left(-\left(\sqrt{v_x^2 + 2\varphi(x)} - V_0\right)^2/2\right)\exp\left(-v_y^2/2\right) \tag{10}$$

According to this solution, the ion VDF in the plane (v_x, v_y) is deformed (become narrower along v_x) during ion acceleration by the DC field. This means that the ion temperature T decreases in the sheath.
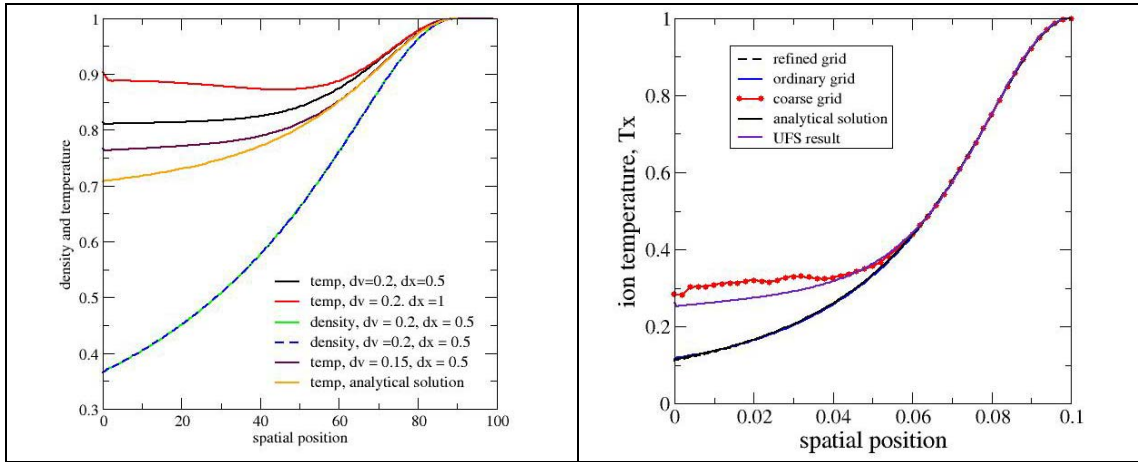

Figure 4.   UFS ion density and temperature from (on the left) for different size of velocity and space mesh. Ion temperature from Shoucri's code and UFS (on the right)

7

Figure 4 (left part) shows the UFS numerical solution for $s_m = 90$, $V_0 = 10$, $A = 8$. This force corresponds to the potential $\varphi(0) = 360$ and the mean velocity is $v(0) = \sqrt{820} = 28.6$. It is seen that even with the spatial mesh of 200 points and velocity mesh of 250 points we can not reproduce the analytical profile of the ion temperature with the UFS code. The right part of Figure 4 shows the temperature profiles obtained with the UFS and S-codes. The UFS code uses second order scheme with van Leer limiter, the S-code uses cubic interpolation. The S-code reproduces analytical result even for (100,120) nodes. The UFS fails even for (200,250) nodes.

Figure 5 shows velocity distributions from S-code and UFS for potential drop 400. The UFS results are for 200 nodes in physical space and 250 nodes in velocity space. The S-results are for (200, 240), (100,120) and (50,60) nodes.

Figure 5.   Ion distribution functions from Shoucri's code (left) and UFS (right).

For $V_0 = 0$, the velocity distribution remains isotropic, and the temperature should be constant in the sheath. Figure 6 shows the electron distribution function at the electrode and temperature distributions from the Shoucri's and UFS codes. The potential drop is –8. The UFS results are for 200 nodes in physical space and 100 nodes in velocity space. The S-results are for 50 nodes in space and 140 nodes in veloci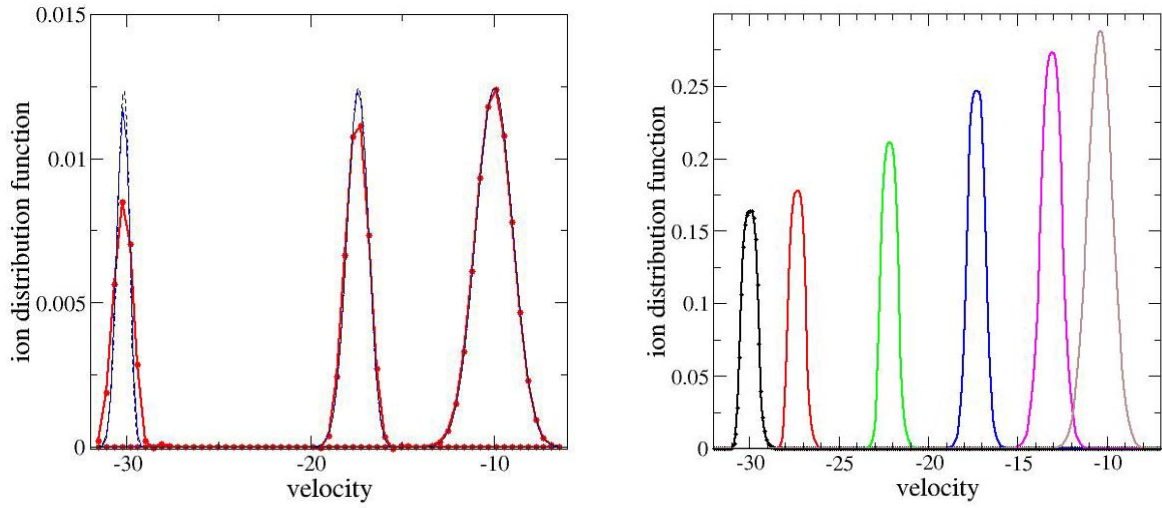ty space. It is seen that the S-code reproduces the expected temperature profile with better accuracy. The temperature drop near the boundary is due to absorption of the fastest electrons at the boundary.
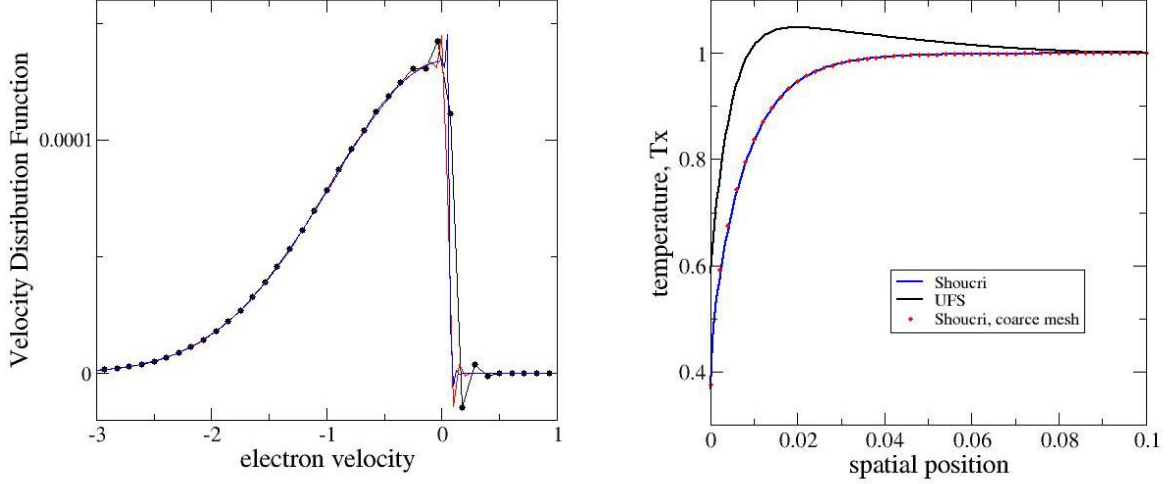
Figure 6.   Electron distribution functions from Shoucri's code at electrode (left) and spatial distribution of electron temperature (right).

2.2   DC boundary layer in collisionless plasma

We have derived analytical expressions for the electron and ion velocity distribution functions in the collisionless DC sheath and verified results of the numerical solution of the Vlasov-Poisson system [15] versus the analytical solution.

The problem statement is described in details in [15]. Briefly, electrons and ions are injected from the right boundary ($x=L$) with given velocity distributions. The boundary at $x=0$ corresponds to floating potential collecting charge. We use dimensionless variables introduced in [15], where space is normalized to the electron Debye length, time is in units of inverse ion plasma frequency, and velocity is in the units of ion acoustic speed, $c_s = \sqrt{T_e/M}$. A surface charge is built up at $x=0$ to equalize electron and ion currents to the wall in a steady state. The problem is characterized by two parameters: the ratio of electron to ion mass, *xmei=m/M*, and the ratio of electron to ion temperatures, $t_{ei} = T_e/T_i$.

In our present simulations, *L*=20, ion time step $\Delta t = 0.01$. We solve electron Vlasov equation with Poisson equation in a sub-cycle with *nturn* steps and the electron time step $\Delta t / nturn$ (with *nturn*=60). The velocity space for electrons $-4/\sqrt{xm_{ei}} < \xi_e < 4/\sqrt{xm_{ei}}$, for ions $-17/\sqrt{t_{ei}} < \xi_i < 0/\sqrt{t_{ei}}$ at $t_{ei} = 30$. The problem reaches a steady state at *t*~10 in less than an hour of computing time. Results shown below are for *t*=20.

Figure 7 shows spatial distributions of particle densities and temperatures for *tei*=30. The electron density drops in the sheath because the electrostatic potential repels the electrons back to plasma. The analytical solution of the Vlasov equation for the electron velocity distribution function has the form

$$f_e(\xi, x) = \begin{cases} \exp(-\varepsilon) & \xi < \sqrt{2\Delta\varphi(x)/xm_{ei}} \\ 0 & \xi > \sqrt{2\Delta\varphi(x)/xm_{ei}} \end{cases} \tag{11}$$

9

where $\varepsilon = \xi^2/2 - \varphi(x)$ is the total energy, $\varphi(x)$ is the electric potential measured in units of T_e, and $\Delta\varphi(x) = \varphi(0) - \varphi(x)$. It is assumed that $\varphi(L) = 0$. The electron temperature is dropped in a vicinity of the wall due to the depletion of electron velocity distribution by fast electrons, which overcome the electrostatic potential barrier and escape to the wall. No electrons reaching the wall return back to plasma, and the electron velocity distribution function is zero at $\xi > \sqrt{2\Delta\varphi(x)/xm_{ei}}$ (see Figure 8).

The ion density drops because the electrostatic field accelerates the ions and their mean velocity increases while the ion current remains constant. The ion velocity distribution can be described by the analytical expression

$$f_i(\xi, x) = \begin{cases} \exp\left(-t_{ei}\left(\sqrt{\xi^2 + 2\varphi(x)} - v_0\right)^2/2\right), & \xi < 0 \\ 0 & \xi > 0 \end{cases} \tag{12}$$

It follows from this expression that the amplitude of the ion distribution remains constant, and the width of $f_i(\xi, x)$ with respect to velocity decreases in the sheath. The decrease of the IVDF width corresponds to decrease of the ion density and temperature $T_{ix}(x)$ in the sheath (see Figure 7).
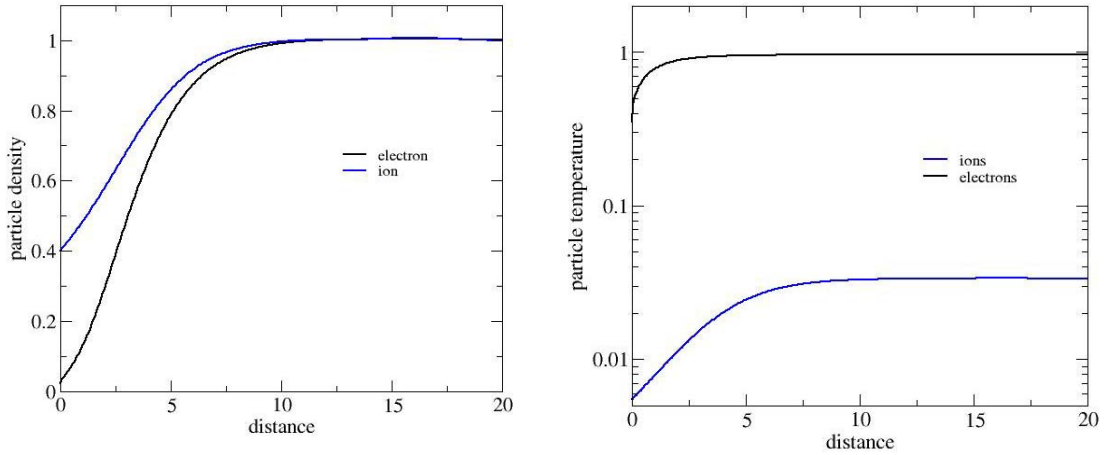
Figure 7.   Particle densities (left) and temperatures (right) for tei=30.
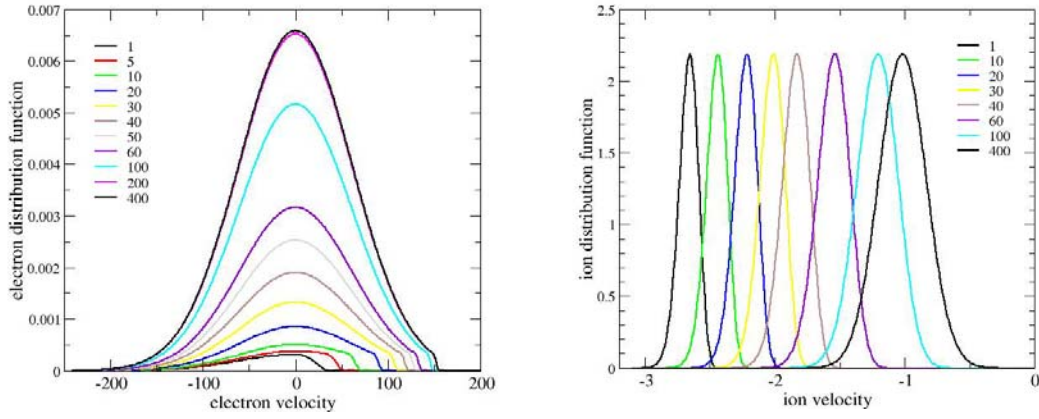
Figure 8.   Electron velocity distributions (left) and ion velocity distributions (right) at different spatial positions for tei=30. Numbers denote spatial mesh points for the total of 400 mesh points.

Figure 9 compares the distribution of density profiles and temperature profiles for *tei*=10 and *tei*=30. It is seen that the sheath width is slightly larger at *tei*=10 compared to *tei*=30.
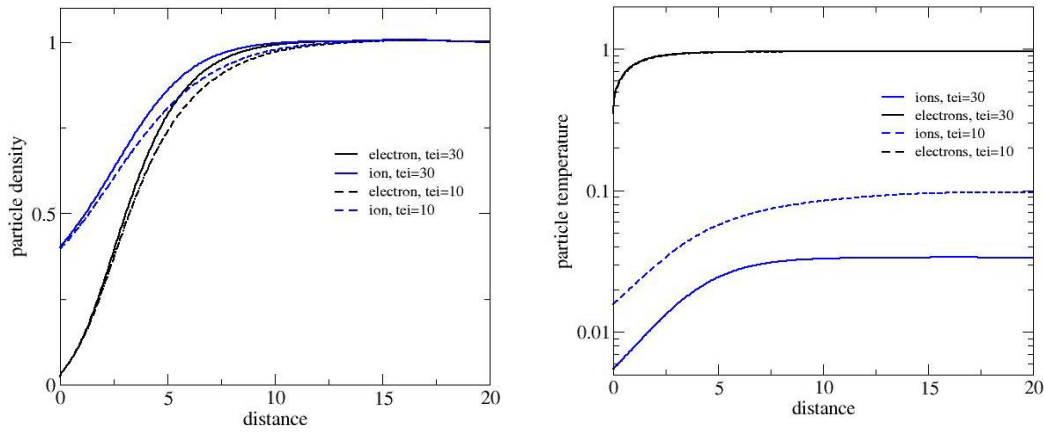
Figure 9. Comparison of density profiles (left) and temperature profiles (right) for tei=10 and tei=30.

Figure 10 shows the distribution functions for Ar, which can be compared with Figure 8 to understand changing of the velocity range with changing *xmei* parameter.
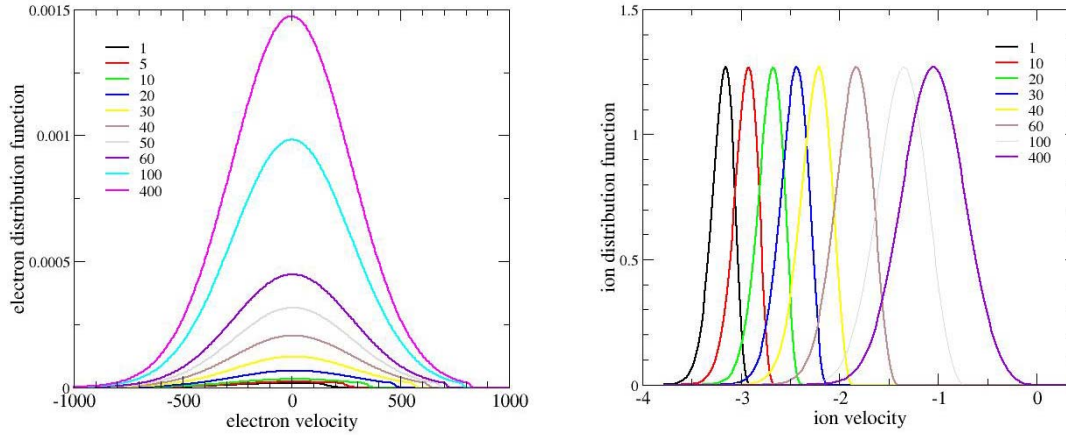
Figure 10. Comparison of density profiles (left) and temperature profiles (right) for tei=10 and tei=30.

Our research described in this section allowed <u>better understanding of particle kinetics</u> in the collisionless DC sheath. The results were reflected in a book chapter [16] submitted for publication.

2.3   Convected Scheme

During Phase I, the academic partner at the University of Wisconsin has tested the Convected Scheme (CS) method for collisionless sheath problems. The CS is a semi-Lagrangian solution to the Boltzmann equation, which offers advantages over standard methods of characteristics in that it naturally conserves density, energy and other variables, locally in phase space. It is believed to be more accurate than fully mesh-based (Eulerian) methods. The CS offers advantages over other methods in the "intermediate" regime where the mean free path is comparable to the spatial scales, due to its ability to, on one hand, take steps up to a fraction of the mean free path, and on the other, provide conservation at each step it takes.

As a first step towards hybrid models, we have set up a self-consistent and time-dependent model for the electron and ion distribution functions in the RF sheath. In Figure 11 we compare CS results for the electron distribution to an analytical solution for a given distribution of the electrostatic potential; very close agreement is obtained. The results are consistent with Figure 8 obtained with the Eulerian Vlasov solver, which is especially revealing when the velocity distributions are plotted versus electron velocity rather than kinetic energy (see Figure 11).
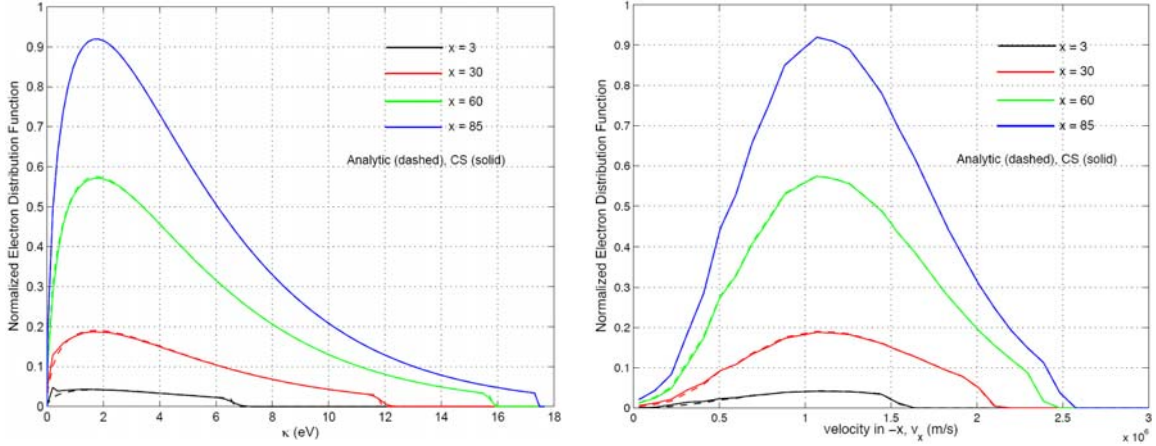
Figure 11   Electron distribution functions plotted versus kinetic energy (left) and velocity (right) for different points inside the sheath.

The time evolution of the ion and electron densities in the collisionless sheath at RF frequency 200 MHz is shown in Figure 12. In these calculations, the electron density follows the Boltzmann law, and the Vlasov equation for ions is solved together with Poisson equation with boundary conditions for the potential $\varphi(0) = \varphi_0 (1 + \cos(\omega t))$ at x=0 and $\varphi(L) = 0$. $\varphi_0 = 200$ V.
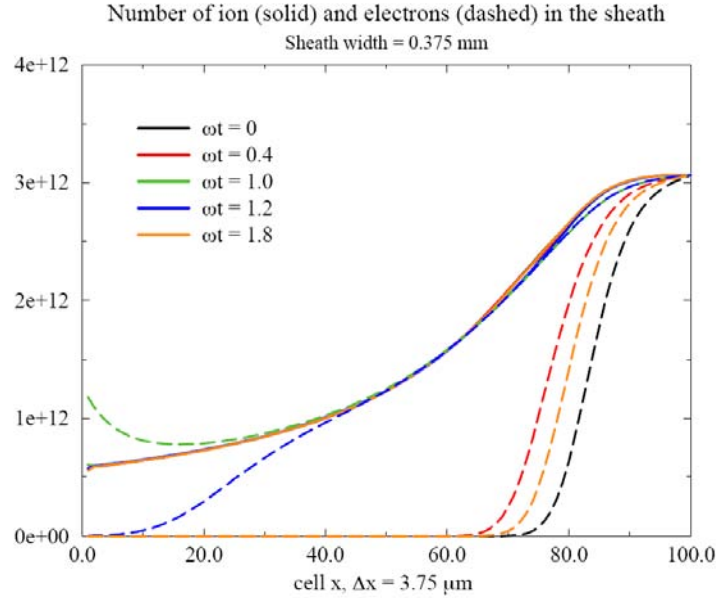
Figure 12   Time evolution of the ion and electron densities in the sheath

In the future, we intend to run kinetic calculations for both the ion and electron distributions in the RF sheath, and develop methods to accelerate simulations taking advantage of the disparity of electron and ion mass. We will then perform analysis of the two sets of results obtained, to ensure that the CS solution for the electron distribution matches that obtained using the simplified relation.

3. BOLTZMANN SOLVER WITH ADAPTIVE MESH IN VELOCITY SPACE

It is known that Lagrangian methods are more efficient than Eulerian methods in terms of computer memory because they use only those parts of phase space where the particles are present. The efficiency of Eulerian kinetic solvers can be increased by using phase functions or adaptive mesh in velocity space. In fact, some people believe that due to high dimension of phase space, adaptive mesh is a must for multi-dimensional kinetic simulations using Euler methods. Octree Cartesian mesh is particularly attractive for this purpose because there are no complex boundaries in velocity space.

We have implemented local Boltzmann solver with adaptive mesh in velocity space for simple types collision terms. The local kinetic equation contains two parts: the transport in velocity space under action of an external force and the collisional part:

$$\frac{\partial f}{\partial t} + \frac{eE(t)}{m}\frac{\partial f}{\partial \xi_x} = S \tag{13}$$

The transport part was implemented (in 2D and 3D velocity space) using the finite volume formulation with second-order accuracy in time and space. The octree/quadtree data structure allowed dynamic grid adaptation. For mapping from one velocity grid to another, second-order accuracy scheme was used. The collisional part depends on the type of the collisional integral. We have implemented so far three types of collision integrals

- the BGK collisional integral
- the charge-exchange collisional integral for ions moving in a parent gas
- the elastic (isotropization) part of the collision integral for electrons collisions with atoms (in the limit $m/M \to 0$).

For the BGK collisional integral, the use of adaptive meshes allowed us to avoid special corrections, which required before for coarse, non-adaptive grids. The isotropization integral for electrons was implemented using a special technique developed in our previous work to correctly treat leaps of particles from one phase cell to another on non-uniform and unstructured grids.

All calculations presented below were very fast, taking from 30 sec to 10-20 min on a 2.2 GHz PC. This is due to the adaptive grid capabilities allowing us to minimize the number of velocity grid points to adequately describe the studied distribution functions.

3.1 BGK Collision Integral

We first tested a collisionless case for a time varying electric field, $E = E_0\cos(\omega t)$. We have confirmed that the density and temperature are conserved with high precision during the simulations, while the mean velocity oscillated with the field frequency ω. Then, the effect of collisions was investigated. The BGK collision term was used in the form $\nu(f_m - f)$ where f_m is a Maxwellian distribution with prescribed density, temperature and mean velocity, and ν is the collision frequency. Figure 13 shows the computational mesh and 2D distribution function in velocity space (ξ_x, ξ_y). Once can see that the velocity grid adapts on the features of the distribution function based on gradient of the velocity distribution function. Figure 14 shows the velocity distributions along ξ_x for $\xi_y = 0$ for two different times. The final distribution function (after about 500 collisional times) has two peaks. These peaks correspond to positions

in velocity space where the particles spend most of the time (where *dE/dt* is small and changing sign).
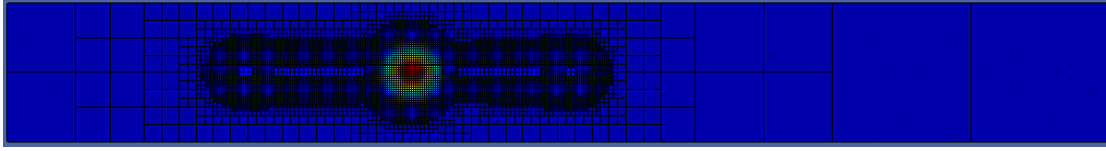

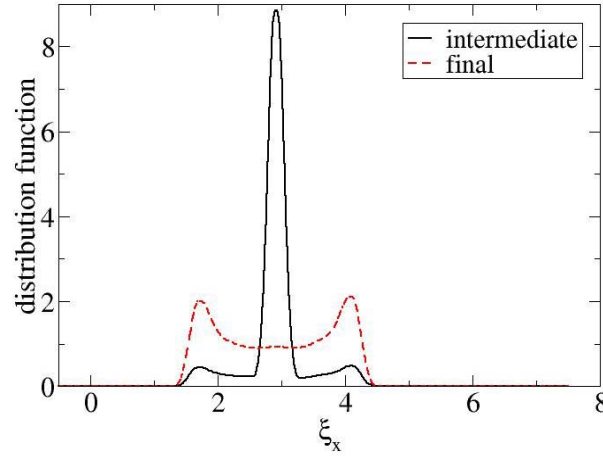*Figure 13.   Instantaneous Computational mesh and velocity distribution (color)*

Figure 14.   The velocity distribution function with respect of ξ_x for $\xi_y = 0$.

Using adaptive mesh in velocity space allows accurate description of the velocity distribution function and its moments. An analytic expression for the mean velocity was obtained in a simple form:

$$u = u_0 \exp(-\nu t) + u_m [1 - \exp(-\nu t)] + E_0 /[\nu^2 + \omega^2][\nu \cos(\omega t) + \omega \sin(\omega t) - \nu \exp(-\nu t)]$$

where u_0 is the initial velocity. The equation for temperature was solved numerically.

The comparison of moments calculated from VDF with analytical results demonstrated very good agreement, thus proving that the numerical scheme is capable of maintaining high accuracy during simulations of long time evolution (here, about 500 collisional times). In addition, we have checked that the implemented BGK collision integral maintains the shape of the distribution function in the ξ_y-direction. The test showed that the T_y temperature remains constant over the simulated time interval with a 2% precision.

3.2   Ions in a DC electric field with charge-exchange collisions

For charge-exchange collisions of ions with a parent gas the collision integral can be written in the form [17]

$$S_i = N \int_{R^3} \left[f(\xi_1)\varphi(\xi) - f(\xi)\varphi(\xi_1) \right] |\xi - \xi_1| \sigma_{ex} d\xi_1 \tag{14}$$

where $\varphi(\xi)$ is a Maxwellian velocity distribution of the background gas atoms with density *N* and temperature *T*, σ_{ex} is a charge exchange collision cross-section.

Consider ions with a mass M injected in DC electric field E and experiencing charge-exchange collisions with a steady background gas. The charge exchange collisions cannot change the velocity distribution orthogonal to the electric field direction. So, the velocity distribution is of the form $f(\xi) = \Phi(\xi_\perp)F(\xi_x)$. The distribution function $F(\xi_x)$ evolves in time until a steady state is reached. The analytical expression for the steady state distribution $F(\xi_x)$ can be obtained in the form

$$F(\xi_x) = C \exp\left(-\frac{NM}{eE} \int_0^{\xi_x} \xi_x \sigma_{ex}(\xi_x) d\xi_x \right) \tag{15}$$

Figure 15 shows results of the numerical solution of the 2D kinetic equation with adaptive mesh in velocity space for the ion distribution function under an applied force of magnitude 4 and charge-exchange collision-frequency of 1. Figure 15 shows the calculated ion distribution function at three moments in time: initial, intermediate and final. One can see the grid adaptation on the features of the distribution function as it evolves in phase space. Figure 16 shows the distribution functions along the $\xi_y = 0$ line for different time moments (left) and distribution functions along $\xi_x = $const lines. One can see that the calculated steady-state distribution function compares well with the analytical solution. In the ξ_y-direction, the distribution function remains a Maxwellian with the temperature of the source function (which represents cold, motionless atoms on which charge-exchange occurs).
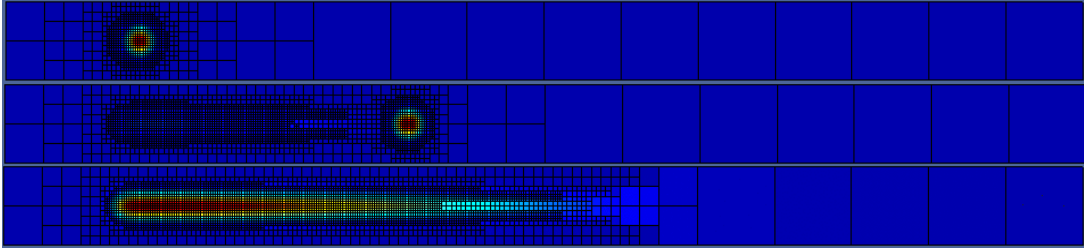
Figure 15.   Ion distribution function at three moments in time: initial, intermediate and final.
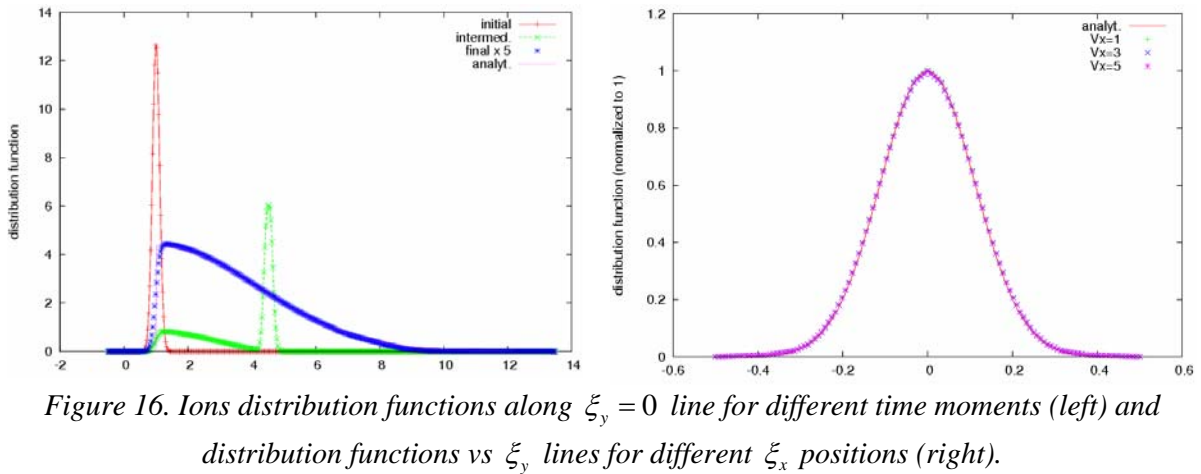
Figure 16. Ions distribution functions along $\xi_y = 0$ line for different time moments (left) and

distribution functions vs ξ_y lines for different ξ_x positions (right).

Figure 17 shows evolution of macroparameters of the simulated ion distribution function in an external field under charge-exchange collisions. One can see that the density is well conserved (variation is less than 0.05%), the velocity and temperatures reach steady state in around 5-6

16

collision times. One can also notice that the temperature (or average energy) in the field direction (here, T_x) becomes about 300 times larger than the transversal one (here, T_y), which itself remains constant (recall that the charge-exchange collision integral does not change the distribution function in the transversal direction). These facts provide evidence of that the numerical scheme based on adaptive mesh is capable of handling such large differences in parameters of the distribution function.

Figure 17.   Evolution of macroparameters of the simulated ion distribution function in an external field under charge-exchange collisions.
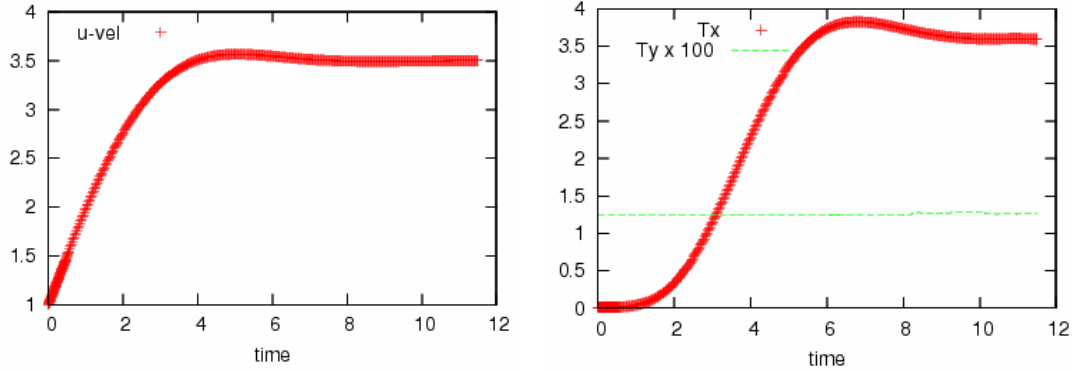
3.3   Electron isotropization under effect of elastic collisions

The ratio of electron to atom mass, $m/M \square 10^{-4}$, is a small parameter of the system. In this case, the Lorentz gas model can be used to describe elastic collisions of electrons with gas molecules. The collision integral is a sum of two terms, $S_e = S_e^0 + S_e^1$. The first term describes momentum relaxation in the limit $m/M \to 0$ (Ref. [18], Eq. 6.1.18)

$$S_e^0 = 4N \int_{S^2} d^3 \mathbf{l} \delta(l^2 + \boldsymbol{\xi} \cdot \mathbf{l}) I(\xi, l) \big[f(\boldsymbol{\xi} + 2\mathbf{l}) - f(\boldsymbol{\xi}) \big] \tag{16}$$

where the vector $\mathbf{l}$ corresponds to the change of $\mathbf{v}$ due to the collision, $\boldsymbol{\xi}' = \boldsymbol{\xi} + \mathbf{l}$. This term vanishes, $S_e^0 = 0$, for any isotropic distribution, since $|\boldsymbol{\xi} + 2\mathbf{l}| = \xi$. The differential scattering cross section $I(\xi, l)$ is determined by the intermolecular interaction potentials. For hard spheres with diameter a, $I(\xi, l) = a^2/4$. The second term, S_e^1, accounts for energy exchange between the light and heavy particles, it can be written in a differential (Fokker-Planck) form.

The integration (16) takes place over a sphere in velocity space and can be alternatively written as

$$S_e^0 = N\mathrm{v} \int_{S^2} \sigma(\xi, |\boldsymbol{\Omega} - \boldsymbol{\Omega}'|) \big[f(\xi, \boldsymbol{\Omega}') - f(\xi, \boldsymbol{\Omega}) \big] d\Omega \tag{17}$$

where $\boldsymbol{\Omega}$ is a velocity angle on a unit sphere S^2 in velocity space, $\boldsymbol{\xi} = \xi \boldsymbol{\Omega}$, and σ is the differential collision cross section, which depends on the initial speed and the angle $\theta = \arccos(\boldsymbol{\Omega} \cdot \boldsymbol{\Omega}')$ between the initial and final electron velocity. When the scattering is close to isotropic $\sigma(\xi, |\boldsymbol{\Omega} - \boldsymbol{\Omega}'|) = \sigma(\xi)$, the integral (17) is further simplified

$$S_e^{el} = -\nu[f(\xi,\Omega) - \int_{S^2} f(\xi,\Omega)d\Omega] \tag{18}$$

where $\nu = N\xi\sigma(\xi)$ is the collision frequency.

This section describes calculation performed with the collision integral (17) for the simplest case of isotropic scattering (918). We first studied two cases without external force.

3.3.1 <u>Isotropization of an initially non-isotropic distribution</u>

In this case the initial distribution function is has an elliptic shape with zero mean velocity and $T_x = 3T_y$. This case is important for testing how the implemented collision integral conserves the moments of the distribution function. The computational grid in velocity space and the initial and final velocity distribution functions are shown in Figure 18. The evolution of the T_x and T_y temperatures calculated from the velocity distribution function is shown in Figure 19.
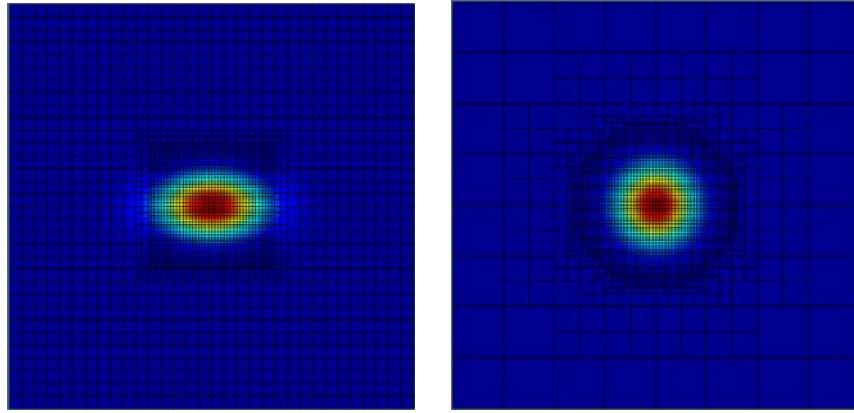

Figure 18.   Initial and final distribution function for case with initially non-isotropic distribution.
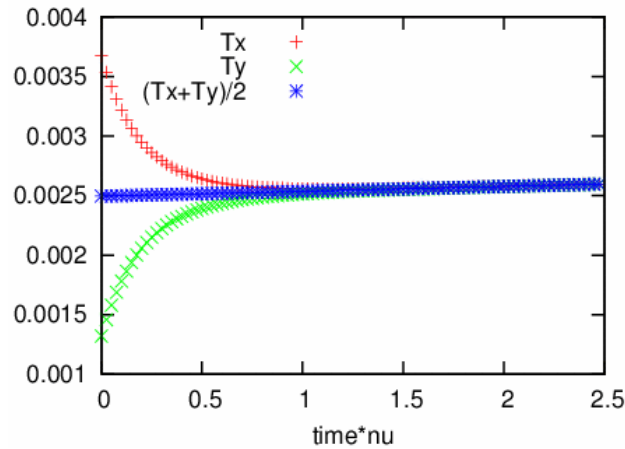
Figure 19.   Time evolution of temperatures for the case with an initially non-isotropic distribution.

3.3.2 <u>The case with initially non-isotropic and shifted distribution without force</u>

In this case, the initial velocity distribution function has non-zero velocity mean velocity, $\xi_x = 0.3$, and temperature $T=0.005$. Figure 20 shows the dynamics of the isotropization process. The corresponding macroparameters are shown in Figure 21. The density is conserved with a machine precision. The mean velocity drops to zero in about two collisional times. The

18

temperatures T_x and T_y evolve towards a single temperature with the same time scale.

Figure 20.   The computational grid and the initial, intermediate and final distribution functions (color) under the action of the isotropization integral.

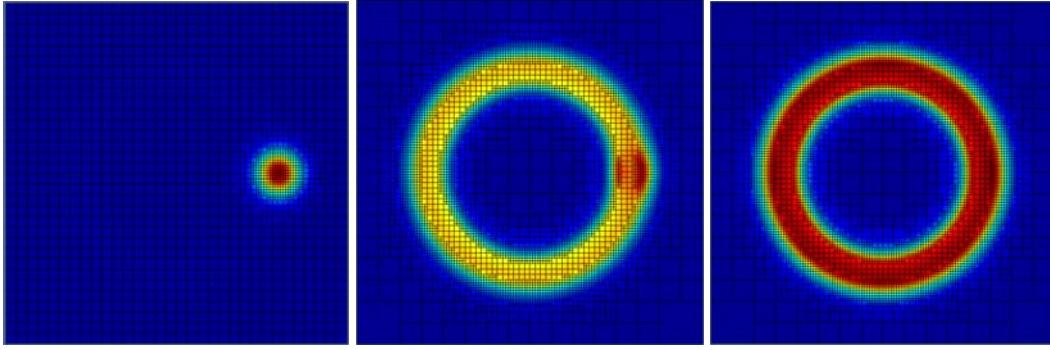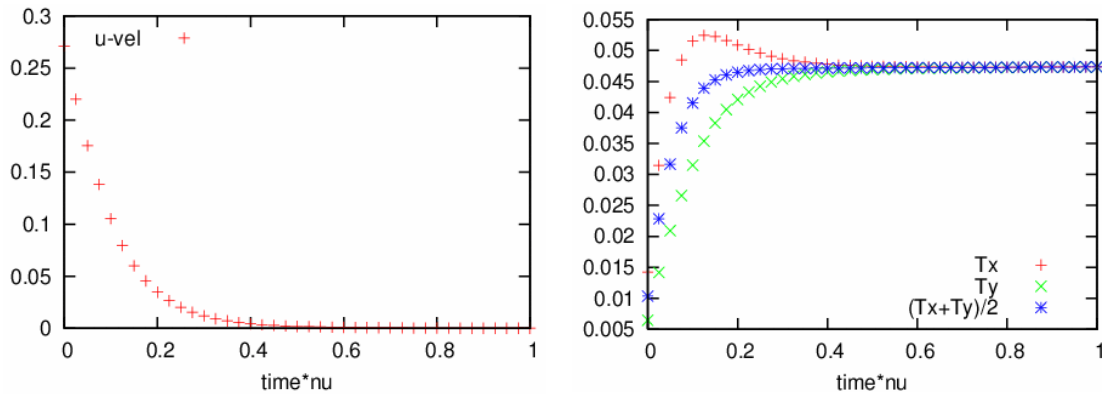*Figure 21.   Time evolution of macroparameters of a distribution function with initial non-zero velocity.*

3.3.3   The case with initially isotropic distribution and force

Finally, a test with a force has been carried out. Figure 22 shows distribution function at three time moments under the action of the isotropization integral (frequency of 1) and in presence of force (amplitude of 0.25). One can see the distribution function moves in the direction of the force and at the same time evolves in the ξ_y-direction under the action of the isotropization integral (along $|\xi|$=const circles). The velocity grid dynamically adapts to the features of the instantaneous distribution function. The temperature (or average energy) grows with time (with slight difference of T_x and T_y), as see in Figure 23. Since there are no energy losses, the temperature will grow indefinitely.
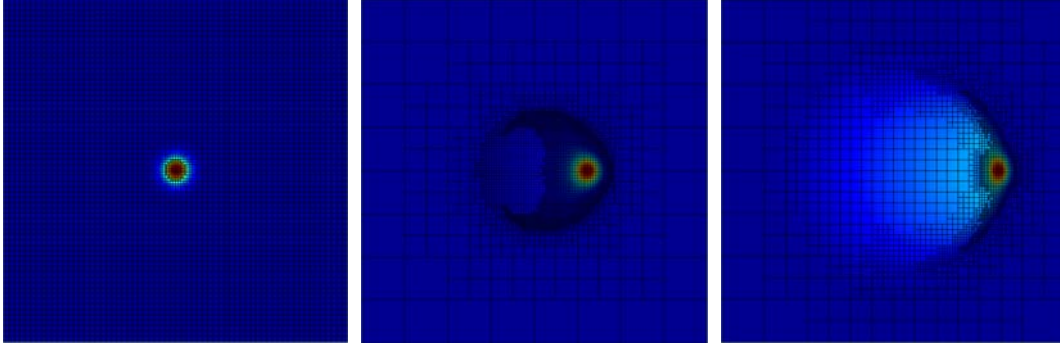
Figure 22.   *Distribution function at three time moments under the action of the isotropization integral and in presence of force.*

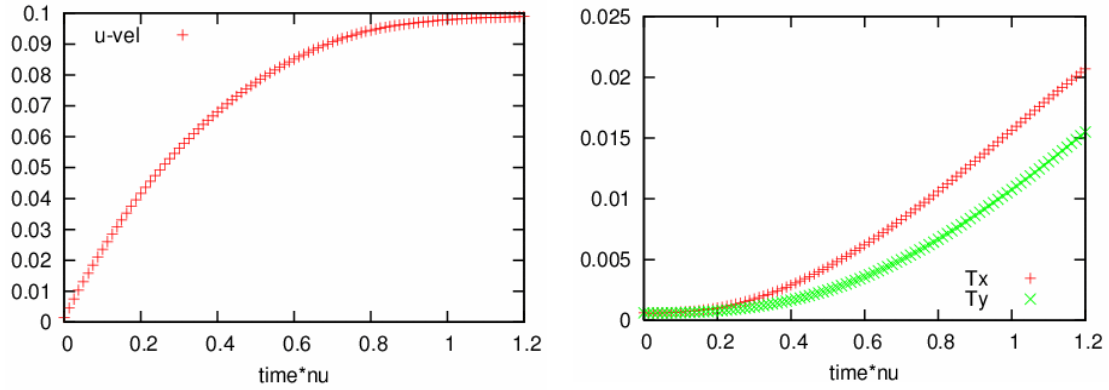*Figure 23.*   *Time evolution of macroparameters of a distribution function under the action of the isotropization integral and in presence of force.*

In order to test the implementation of the isotropization integral, we have carried a test with force of a coarse grid. The results with Maxlevel=7 show practically no difference with those on a fine grid (Maxlevel=8). The simulation with a Maxlevel=7 took only 30 sec of computing time.

4.   FLUID PLASMA MODELS

The fluid models of plasma utilize two (density and velocity) or three (density, velocity, and temperature) equations for electrons and ions coupled to electromagnetic solvers. During Phase I, we advanced fluid plasma models in two directions.

4.1   Basic Plasma Solver with Dynamically Adaptive Mesh

We developed new capabilities for fluid plasma simulations with dynamically adaptive Cartesian mesh using simple plasma model. The model contains transport/ionization of electrons and ions coupled to the Poisson equation for the electric field. This model is appropriate for simulation of collision-dominated high-pressure discharges. Our computational tool is unique in several aspects: i) plasma equations are solved with dynamically adaptive quadtree/octree Cartesian mesh, which provides an excellent compromise between the flexibility of unstructured meshes and the computational efficiency of structured meshes, ii) complex boundaries are represented using the volume-of-fluid approach enabling simulations of curved electrodes, iii) large dynamic range of grid refinement/coarsening (up to 10-12 levels) provides high resolution of the streamer fronts.

The efficient and accurate technique for grid refinement/coarsening is very important for simulations of streamers with dynamically adaptive mesh. It was found empirically that for reliable results, the following criteria had to be used:

$$\left| n_{e,i}(r_j) - n_{e,i}(r_{j+1}) \right| < 0.05 \max(n_{e,j}) \text{ and } n_{e,i}(r_j) / n_{e,i}(r_{j+1}) < 2$$

$$\left| \mathbf{E}(r_j) \right| / \left| \mathbf{E}(r_{j+1}) \right| < 2 \text{ and } v_i(r_j) / v_i(r_{j+1}) < 5$$

where n_e and n_i are the electron and ion densities, $\mathbf{E}$ is the electric field and v_i is the ionization frequency, and r_j and r_{j+1} denote neighboring cells.

An example of 3D simulations of streamer development from an initial perturbation is shown in Figure 24a. No branching of streamers has been observed in our simulations. No streamers develop in high electric fields, dumb-bell shape structures appear instead. Figure 24b shows 2D axi-symmetric streamer development near a high-voltage needle-like cathode. The streamer propagates with a velocity by an order of magnitude higher than the electron drift velocity in the highest electric field in the gap. The calculated velocity agrees with classical estimates for the fast streamer velocity. Figure 24c illustrates streamer development from two spatially separated avalanches. Both negative and positive streamers expand with velocities higher than the electron drift velocity. The negative streamer velocity is 3 times higher than the drift velocity, the positive streamer velocity is about 2 drift velocities. The neighbor streamers get closer during their development; the field increases in the gap between the streamer tips, and ionization takes place along the line connecting the positive and negative tips.

In all cases, the calculated fields near the streamer tips were of the order of the critical field corresponding to saturation of the ionization frequency with respect to the field strength. This implies that non-local ionization should play an important role in these regions.
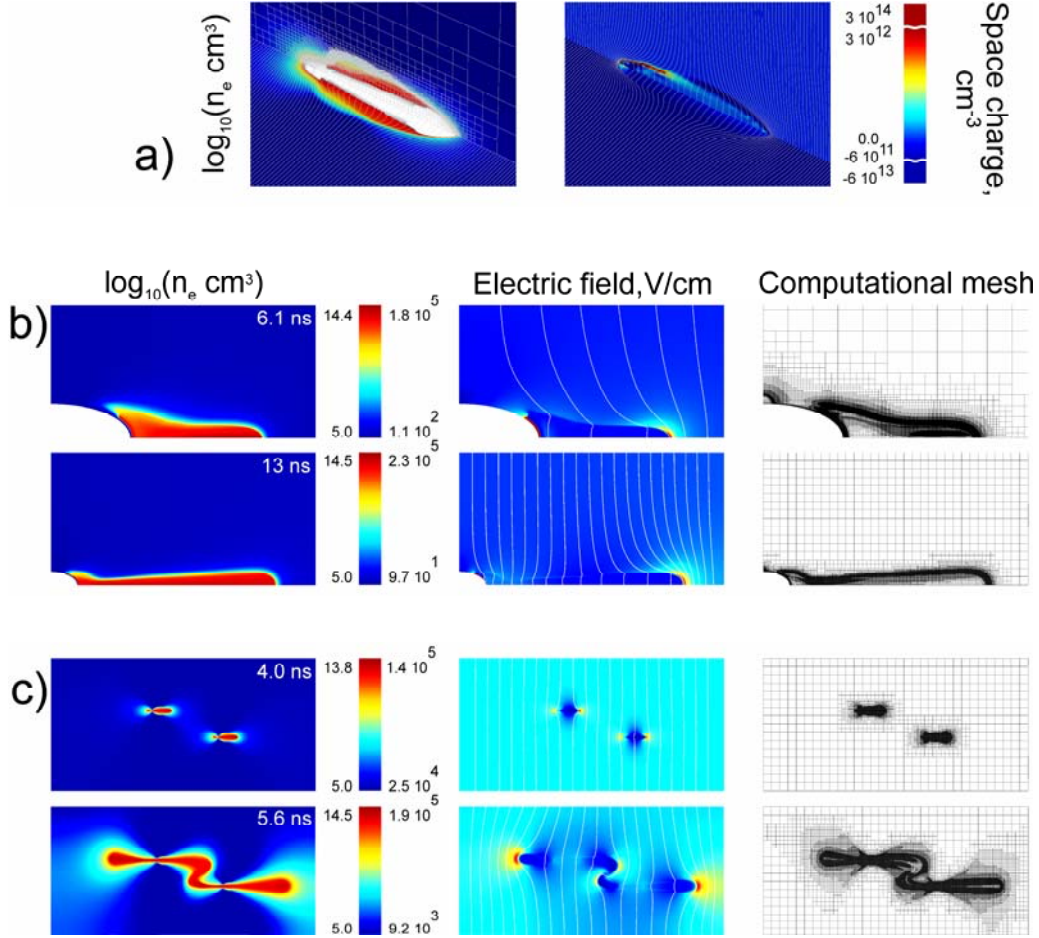
Figure 24.   a) 3D simulation of a streamer development from an initial perturbation in N_2: p=400 Torr, E=34 kV/cm, b) 2D axi-symmetric simulation of streamer development between a needle-like elliptic cathode (size 2×1 cm) and a flat anode: p=760 Torr, cathode potential -600 kV, c) interaction of two avalanches during their transition to streamers: p=760 Torr, E=65 kV/cm, computational domain 2×1 cm and initial plasma density 5×10^{10} cm^{-3}.

4.2   <u>Adding Forces in the gas kinetic continuum solvers</u>

We have studied numerical algorithms associated with external forces in the gas kinetic Euler and Navier-Stokes solvers. The implementation of forces in gas kinetic schemes and difficulties associated with "numerical heating" are described in Ref. [19]. For tackling this effect, we used the approach proposed in Ref. [20].

In order to test different algorithms, we have considered a problem of a stationary gas in periodic field with potential $\varphi = -\varphi_0 \frac{L}{2\pi} \sin(\frac{2\pi x}{L})$. The analytical solution to this problem corresponds to zero mean velocity, constant gas temperature, and the density distributed according to the Maxwell-Boltzmann relation ($\rho \sim \exp(-\phi/T)$). The most difficult part in this benchmark test is to achieve small velocity and constant temperature. We have used 3 different algorithms to account for the force terms in our NS solver: the first approach uses a limiter (Van-Leer), the second case is without a limiter and the third one is from Ref. [19]), which accounts for the terms with the force inside the distribution function. The results using these

methods are compared in Figure 25. One can see that for the third method, the smallest velocity values could be obtained and the temperature is close to a constant. The results are very encouraging since they show that it is possible to achieve high precision by using the appropriate numerical implementation for the force term in gas kinetic schemes. This approach is planned for future coupling of the Boltzmann solution with the NS solution in the presence of forces in realistic plasma systems.
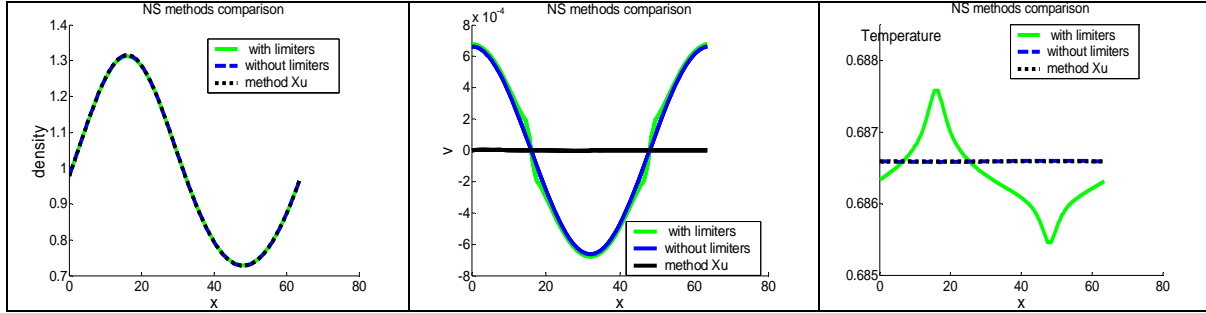

Figure 25.   Density, velocity and temperature for the problem of a gas in a periodic gravitational field.

5.   CONCLUSION

During Phase I, we have investigated methods of Renormalization Group and Slow Invariant Manifolds in application to plasma modeling. Using the symmetry group for the Vlasov-Maxwell system, we obtained exact solutions for the dynamics of boundary layer in collisionless plasma. The interpretation of the solutions in terms of invariants of the group transformation and invariant manifolds was achieved – the particle distribution functions were related to invariants of the group transformation. The road towards obtaining approximate symmetries due to small parameter (electron/ion mass ratio) in the plasma was identified. We prepared detailed work plan for further development and application of this methodology for weakly ionized collisional plasmas in Phase II. We have analyzed and tested several numerical methods of solving the Vlasov and Boltzmann kinetic equations for charged particles in weakly ionized plasma. We found that cubic spline interpolation provides superior results compared to the second order scheme with van Leer limiter. The Eulerian Vlasov solver with cubit interpolation reproduced analytical results for the shape of the velocity distribution function with high accuracy using a reasonable number of mesh points. We have evaluated numerical methods of solving hydrodynamic plasma equations for different types of computational grid. We have developed a minimal plasma solver with dynamically adaptive mesh capabilities and demonstrated this solver for the problem of streamer development in different electric fields. We have submitted a paper to IEEE Transactions on Plasma Science entitled "Streamer Simulations with Dynamically Adaptive Cartesian Mesh", which was accepted for publication.

6.   REFERENCES

1   S-I Ei, K.Fujii and T.Kunihiro, Renormalization-group method for reduction of evolution equations. Invariant Manifolds and Envelopes, Ann. Phys. 280 (2000) 236

2   O.Pashko and Y.Oono, The Boltzmann equation as a renormalization group equation, Int. J. Mod. Phys. B 14 (2000) 555-561

3   T.Kunihiro and K.Tsumura, Application of the renormalization group method to the reduction of transport equations, J. Phys. A 39 (2006) 8089

4   A.N.Gorban, I.V.Carlin, A.Yu Zinoviev, Constructive methods of invariant manifolds for kinetic equations, Phys. Reports 396 (2004) 197-403

5   J. Veysey II and N.Gldenfeld, Simple viscous flows: From boundary layers to the renormalization group, Rev. Mod. Phys. 79 (2007) 883

6   A.N.Gorban, I.V.Karlin, Invariant Manifolds for physical and chemical kinetics, Lect. Notes Phys. 660 (Springer, 2005)

7   A.N.Gorban, Basic Types of Coarse-Graining, in Model Reduction and Coarse-Graining Approaches for Multiscale Phenomena, Edited by A. N. Gorban, N. K. Kazantzis, I.G. Kevrekidis, H. C. Öttinger, C. Theodoropoulos, Springer (2006)

8   V.I.Kolobov, Fokker-Planck modeling of electron kinetics in plasmas and semiconductors, Comp. Mater. Science 28 (2003) 302

9   L.D.Tsendin, Physics of Gas Discharges, in press (2008) (in Russian)

10   U.Kortshagen and L.D.Tsendin, *Electron kinetics and applications of glow discharges*, Edited by U.Kortshagen and L.D.Tsendin, NATO ASI Series B: Physics vol. 367, Plenum Press (1998)

11   V.L.Saveliev and K.Nanbu, Collision group and renormalization of the Boltzmann collision integral, Phys. Rev. E 65 (2002) 051205

12   Kolobov, V.I., Arslanbekov, R.R., Aristov, V.V., Frolova, A.A., Zabelok, S.A.: Unified solver for rarefied and continuum flows with adaptive mesh and algorithm refinement, J. Comput. Phys. 223, 589 (2007)

13   M.Shoucri, The Method of Characteristics for the Numerical Solution of Hyperbolic Differential Equations, in Computer Physics Research Trends (2007)

14   W.N.G. Hitchon, Plasma Processes for Semiconductor Fabrication, Cambridge Uni. Press (1999)

15   M.Shoucri, The numerical solution of the kinetic sheath using a Eulerian Vlasov code, Jap. J. Apll. Phys 46, 3045-3051 (2007)

16   M.Shoucri, The application of the method of characteristics for the numerical solution of hyperbolic differential equations, in press (2008)

17   B.M.Smirnov, Physics of Weakly-Ionized Gases: Problems and Solutions, (1982)

18   P.P.J.M.Schram, Kinetic Theory of Gases and Plasmas, Springer (1991)

19   C.T. Tian, K. Xu, K.L. Chan, L.C. Deng, A three-dimensional multidimensional gas-kinetic scheme for the Navier-Stokes equations under gravitational fields, J. Comp. Phys. 2007

20   A. Slyz and K.H. Prendergast, Time-independent gravitational fields in the BGK scheme for hydrodynamics, Astron. Astrophys. Suppl. Ser. 139, 199 (1999)